

The halo mass function from the dark ages through the present day[†]

Darren S. Reed¹ [†], Richard Bower¹, Carlos S. Frenk¹,
 Adrian Jenkins¹, and Tom Theuns^{1,2}

¹*Institute for Computational Cosmology, Dept. of Physics, University of Durham, South Road, Durham DH1 3LE, UK*

²*Dept. of Physics, Univ. of Antwerp, Campus Groenenborger, Groenenborgerlaan 171, B-2020 Antwerp, Belgium*

arXiv:astro-ph/0607150v2 7 Jul 2006

22 February 2019

ABSTRACT

We use an array of high-resolution N-body simulations to determine the mass function of dark matter haloes at redshifts 10–30. We develop a new method for compensating for the effects of finite simulation volume that allows us to find an approximation to the true “global” mass function. By simulating a wide range of volumes at different mass resolution, we calculate the abundance of haloes of mass $10^{5–12} h^{-1} M_{\odot}$. This enables us to predict accurately the abundance of the haloes that host the sources that reionize the universe. In particular, we focus on the small mass haloes ($\gtrsim 10^{5.5–6} h^{-1} M_{\odot}$) likely to harbour population III stars where gas cools by molecular hydrogen emission, early galaxies in which baryons cool by atomic hydrogen emission at virial temperature of $\sim 10^4$ K ($\sim 10^{7.5–8} h^{-1} M_{\odot}$), and massive galaxies that may be observable at redshift ~ 10 . When we combine our data with simulations that include high mass halos at low redshift, we find that the best fit to the halo mass function depends not only on linear overdensity, as is commonly assumed in analytic models, but also upon the slope of the linear power spectrum at the scale of the halo mass. The Press-Schechter model gives a poor fit to the halo mass function at all epochs; the Sheth-Tormen model gives a better match to the simulations, but still overpredicts the abundance of rare objects at all times by up to 50%. Finally, we consider the consequences of the recently released WMAP 3-year cosmological parameters. These lead to much less structure at high redshift, reducing the number of $z = 10$ “mini-haloes” by about one third and the number of $z = 30$ galaxy hosts by nearly three orders of magnitude.

Key words: galaxies: haloes – galaxies: formation – methods: N-body simulations – cosmology: theory – cosmology: dark matter

1 INTRODUCTION

The numbers of haloes in the high redshift universe are critical for determining the numbers of stars and galaxies at high redshift, for understanding reionization, and for guiding observational campaigns designed to search for the first stars and galaxies. The reionization of the universe is thought to be caused by some combination of metal-free stars, early galaxies and accreting black holes (see e.g. Bromm & Larson 2004; Ciardi & Ferrara 2005; Reed et al. 2005 and references therein), all of which are expected to lie in dark matter haloes, the numbers of which are, to date, highly uncertain

at these early times. This paper presents an array of cosmological simulations of a wide range of volumes with the aim of determining the numbers of high redshift haloes over the entire mass range that is expected to host luminous sources in the high redshift universe.

The first galaxies are expected to form within haloes of sufficiently high virial temperature to allow efficient cooling by atomic hydrogen via collisionally induced emission processes, which become strong at temperatures of $\sim 10^4$ K, providing the possibility of efficient star formation. Haloes of mass $\sim 10^8 \times [10/(1+z)^{3/2}] h^{-1} M_{\odot}$ have the required virial temperatures to host galaxies. Haloes with virial temperatures less than the threshold for atomic hydrogen line cooling, but larger than $\sim 2,000$ K, often referred to as “mini-haloes”, have the potential to host metal-free (population

[†] Code to reproduce this mass function can be downloaded at <http://icc.dur.ac.uk/~reed/genmf.html>

[†] Email: d.s.reed@durham.ac.uk

III) stars that form from gas cooled through the production of H₂ and the resulting collisionally-excited line emission. The first stars in the universe are expected to form within such mini-haloes, which have masses as small as $\sim 10^{5-6} h^{-1} M_{\odot}$ at redshifts of $\sim 10-50$. The inability of collapsing H₂-cooled gas to fragment to small masses, demonstrated in pioneering simulations by Abel, Bryan, & Norman (2000, 2002) and by Bromm, Coppi, & Larson 1999, 2002), suggests that these first stars will be very massive ($\gtrsim 100 M_{\odot}$), luminous, and short lived, and will thus have dramatic effects on their surroundings. These population III stars begin the process of enriching the universe with heavy elements, and are expected to have an important impact (directly or indirectly) on reionization.

Early estimates of the numbers of haloes in the pre-reionized and the reionizing universe have relied upon analytic arguments such as the Press & Schechter (1974) formalism or the later Sheth & Tormen (1999; S-T) function. For halos at very high redshifts, which form from rare fluctuations in the density field, these analytic methods are in poor agreement with each other. At lower redshifts, halo numbers have been extensively studied using N-body simulations of large volumes. Simulations by Jenkins et al. (2001) show that the mass function of dark matter haloes in the mass range from galaxies to clusters is reasonably well described by the Sheth & Tormen (S-T, 1999) analytic function out to redshift 5, although with some suppression at high masses. Jenkins et al. proposed an analytic fitting formula for the “universal” mass function found in their simulations. Warren et al. (2005) used a suite of simulations to measure the redshift zero mass function to high precision. Reed et al. (2003) used higher resolution simulations to show that the broad agreement with the S-T function persists down to dwarf scales and to $z = 10$, a result that was confirmed by the larger “Millennium” simulation of Springel et al. (2005). However, at $z \simeq 15$, Reed et al. (2003) also found fewer haloes than predicted by the S-T function. These results indicate that current analytic predictions of halo numbers are inaccurate at high redshift and demonstrate the need for N-body studies to determine the mass function at earlier times.

Early attempts to simulate the formation of dark matter halos in the young universe suffered from effects resulting from the finite box sizes of the simulations, as noted by (e.g. White & Springel 2000; Barkana & Loeb 2004). Recently Schneider et al. (2005) have modeled haloes large enough to host galaxies using PINOCCHIO (Monaco et al. 2002; Monaco, Theuns, & Taffoni 2002), a code that predicts mass merger histories given a linear density fluctuation field. More directly, Heitmann et al. (2006) used N-body simulations to show that haloes large enough to cool via atomic hydrogen transitions, and thus with the potential to host galaxies at redshifts 10 - 20, are well fit by the Warren et al. mass function, with the largest haloes suppressed relative to the S-T function by an amount consistent with that seen in Reed et al. (2003).

Formation of the first haloes large enough to host galaxies occurs as early as $z \sim 35$ (e.g. Gao et al. 2005; Reed et al. 2005), much earlier than the epochs at which the mass function has been calculated directly. The abundance of smaller haloes, capable of hosting population III stars, but too cool for atomic cooling, remains poorly constrained

by numerical simulations. The major difficulty is the computational challenge of performing simulations with very high mass resolution within a volume that is large enough to sample fully the cosmological mass perturbation spectrum. At high redshifts, the effects of finite box size become particularly important because the haloes to be sampled represent rare fluctuations in the linear fluctuation spectrum. Since the mass function is steep, the numbers of such rare haloes are particularly sensitive to large scale, low amplitude density fluctuations. Finite box size effects worsen as one attempts to simulate the smaller volumes needed to resolve lower mass haloes because fluctuations on the scale of the box become comparable to those on the scale of the halo. In Λ CDM cosmologies with spectral slope parameter $n_s = 1$, the effective, local spectral index of the perturbation spectrum, n_{eff} , approaches -3 on the smallest scales, implying that fluctuations on a broad range of scales have similar amplitude (see further discussion in § 2). As a result, proper modelling of the power on scales much larger than the scale of the halo is important. Simulations of small haloes must therefore have a large dynamic range in order to model accurately all of the fluctuations that determine the formation and evolution of a halo.

Several authors have estimated the effect of the finite simulation box size on the halo mass function using techniques based on assuming a simple cutoff in the power spectrum of density fluctuations on scales larger than the box length (Barkana & Loeb 2004; Bagla & Ray 2005; Power & Knebe 2005; Bagla & Prasad 2006). While these techniques are able to account for the missing large-scale power, they do not account for cosmic variance, i.e. the run-to-run variations introduced by the finite sampling of density modes, particularly at scales near the box size (e.g. Sirko 2005). Since the density field is derived from a set of discrete Fourier modes with maximum wavelength equal to the boxsize, the power at the largest wavelengths is determined by only a small number of realized modes. As a result, each random realization of a simulation volume produces different large-scale structures. We introduce a technique, built upon ideas presented in Sirko (2005), that takes into account the finite simulation volume by considering the power spectrum specific to each individual simulation, as computed from the particle positions in the initial conditions of each realization. This allows the simulated halo mass function to be corrected explicitly for the lack of large-scale power and for the finite number of modes in a given realization, providing a means of estimating the global mass function from a simulation of limited volume.

In order to verify the ability of this technique to account for finite volume affects, we perform simulations of a wide, but closely spaced range of volumes, which results in large overlaps in redshift and in the range of resolved halo masses in different simulations. The agreement of the inferred mass functions in the regimes where halo masses overlap allows us to verify the finite volume correction, and also allows us to rule out resolution dependencies of our results. Multiple realizations of a single volume at identical resolution then test how well the correction to the inferred mass function is able to minimize the effects of cosmic variance.

The strategy of this paper is to model directly the haloes relevant to studies of star and galaxy formation in the pre-reionized and the reionizing universe using a series of N-body

simulations of a wide range of box sizes and mass resolutions. Our simulations are designed to extend the mass function to smaller masses and higher redshifts, covering a mass range of 10^5 to $10^{12} h^{-1} M_\odot$, at redshifts 10 to 30, and we supplement them with low redshift data taken from other studies. This extends the mass function down to masses small enough to include the “mini-haloes” capable only of hosting stars formed via H₂-cooling, and determines more precisely the mass function of larger haloes which can host galaxies. In § 2, we discuss our suite of simulations of varying box sizes and resolutions, and we detail our method for correcting for finite volume effects. In § 3, we demonstrate the effectiveness of our techniques for correcting for finite volume and cosmic variance. We then present our mass function and compare it to previous works. In § 4, we consider the dependence of the mass function on cosmological parameters in the light of the recent WMAP third year results (Spergel et al. 2006). In § 5, we discuss some implications of our mass function for astrophysical models that rely on the mass function of high redshift haloes. Finally, our conclusions are summarised in § 6.

Except when otherwise indicated, we assume throughout a flat Λ CDM model with the following cosmological parameters, which are consistent with the combined first year WMAP/2dFGRS results (Spergel et al. 2003): matter density, $\Omega_m = 0.25$; dark energy density, $\Omega_\Lambda = 0.75$; baryon density, $\Omega_{\text{baryon}} = 0.045$; fluctuation amplitude, $\sigma_8 = 0.9$; Hubble constant $h = 0.73$ (in units of $100 \text{ km s}^{-1} \text{ Mpc}^{-1}$); and no tilt (i.e. a primordial spectral index of 1). Note that our results should, in principle, be scalable to other values of cosmological parameters.

2 TECHNIQUES

2.1 The simulations

We use the parallel gravity solver L-Gadget2 (Springel et al. 2005) to follow the evolution of dark matter in a number of realizations of different cosmological volumes. Table 1 lists all our simulations and the numerical parameters used. The highest resolution simulations have particle mass equal to $10^3 h^{-1} M_\odot$ and resolve haloes to redshifts as high as 30. Our new simulation volumes range from 1 to $100 h^{-1} \text{Mpc}$ on a side. For these runs, the cell size of the mesh used by L-Gadget2 in the PM portion of the Tree-PM force algorithm to compute long range gravitational forces is equal to one half the mean particle spacing. We also include results of the $500 h^{-1} \text{Mpc}$ “Millennium run” (Springel et al. 2005). For low redshift haloes, we include analysis of the $1340 h^{-1} \text{Mpc}$ run by Angulo et al. (2006, in preparation), and the $3 h^{-1} \text{Gpc}$ “Hubble volume”, which has $\Omega_m = 0.3$, $\Omega_\Lambda = 0.7$, and $\sigma_8 = 0.9$, was run using HYDRA (Couchman, Thomas & Pearce 1995; Pearce & Couchman 1997), and uses the Bond & Efstathiou (1984) transfer function (see Colberg et al. 2000; Jenkins et al. 2001 for details). We have verified the robustness of our results to the choice of run parameters by varying individually the starting redshift (z_{start}), fractional force accuracy ($\Delta_{\text{force acc}} = 0.005$), softening length (r_{soft}), and maximum allowed timestep ($\Delta_t \equiv \Delta \ln(1+z)^{-1}$); these tests are detailed in the appendix.

Initial conditions for runs with boxlength of $50 h^{-1} \text{Mpc}$

Table 1. Simulation parameters. N_{runs} random realizations of cubical volumes of side L_{box} were simulated, from redshift z_{start} to z_{fin} . N_{part} particles of mass M_{part} and gravitational force softening length r_{soft} were employed.

N_{runs}	L_{box} $h^{-1} \text{Mpc}$	M_{part} $h^{-1} M_\odot$	N_{part}	z_{fin}	z_{start}	r_{soft} $h^{-1} \text{kpc}$
11	1.0	1.1×10^3	400^3	10	299	0.125
1	2.5	1.1×10^3	1000^3	10	299	0.125
3	2.5	1.1×10^3	1000^3	30	299	0.125
1	2.5	8.7×10^3	500^3	10	299	0.25
1	2.5	1.4×10^5	200^3	10	299	0.625
1	4.64	1.1×10^5	400^3	10	249	0.58
2	11.6	1.1×10^5	1000^3	10	249	0.58
1	20	8.7×10^6	400^3	10	249	2.5
2	50	8.7×10^6	1000^3	10	299	2.4
1	100	9.5×10^7	900^3	10	149	2.4
1	500 [†]	8.6×10^8	2160^3	0	127	5.0
1	1340 ^{††}	5.5×10^{10}	1448^3	0	63	20
1	3000 ^{†††}	2.2×10^{12}	1000^3	0	29	100

[†] “Millennium” run (Springel et al. 2005)

^{††} Angulo et al. (2006)

^{†††} “Hubble Volume” (Colberg et al. 2000; Jenkins et al. 2001)

or smaller were created using the CMBFAST transfer function (Seljak & Zaldarriaga 1996) as follows. Traditionally, the initial conditions are generated from a transfer function calculated at $z = 0$ and extrapolated to the initial redshift using linear theory. However, in order to avoid a high wavenumber (k) feature¹ in the CMBFAST $z = 0$ transfer function, our adopted transfer function consists of the $z = 0$ transfer function for small k spliced together at $k = 1 h^{-1} \text{Mpc}$ with a high redshift ($z = 599$) transfer function for large k . Power is matched on either side of the splice. The location of the splice is chosen to be at a point where the shape of the transfer function has essentially no redshift dependence, thereby ensuring continuity of spectral slope. We use a combined mass-weighted dark matter plus baryon transfer function. The $100 h^{-1} \text{Mpc}$ run and the $1340 h^{-1} \text{Mpc}$ runs both used the transfer function used for the Millennium simulation, which is detailed in Springel et al. (2006).

Our virialized haloes are identified using the *friends-of-friends* (FOF) (Davis et al. 1985) algorithm linking all neighbouring particles separated by less than 0.2 times the mean inter-particle separation. We compare with haloes identified using the *spherical-overdensity* (SO) technique in the appendix. Throughout the paper, we consider only haloes resolved with at least 100 particles, a limit that produces a robust mass function, which we show in the appendix.

¹ We noticed a feature in the CMBFAST transfer function at $k \sim 10^{2.5} h^{-1} \text{Mpc}$, where the slope steepens for approximately a decade in k , resulting in a power spectrum that briefly becomes steeper than the theoretical asymptotic minimum slope of k^{-3} at the smallest scales $n_s = 1$. This unexpected feature is not present in high redshift ($z \gg 100$) computations of the CMBFAST transfer function.

2.2 The mass function

In the Press & Schechter (1974; P-S) formalism, mass within a sphere will collapse to form a halo when the overdensity rises above a critical value, δ_c . The mass function of collapsed objects at any time is then determined by the rms variance of mass within spheres, $\sigma^2(M, z)$. The underlying principle implemented in P-S theory is that the fraction of collapsed mass depends solely on the rms linear overdensity, is invariant with redshift, and has only an indirect dependence on cosmology or initial conditions through the variance of the linear power spectrum, $P(k)$, which depends on the cosmological parameters. For an infinite volume,

$$\sigma_\infty^2(M, z) = \frac{b^2(z)}{2\pi^2} \int_0^\infty k^2 P(k) W^2(k; M) dk, \quad (1)$$

where $W(k; M)$ is the Fourier-space top-hat filter, and $b(z)$ is the growth factor of linear perturbations normalized to unity at $z = 0$ (Peebles 1993). Using gaussian statistics, one can then show that the fraction of material contained in collapsed objects per unit $\ln \sigma^{-1}$ should be given by the Press-Schechter mass function:

$$f_{\text{P-S}}(\sigma) = \sqrt{\frac{2}{\pi}} \frac{\delta_c}{\sigma} \exp\left[-\frac{\delta_c^2}{2\sigma^2}\right], \quad (2)$$

where $\delta_c = 1.68647$. All mass is contained in collapsed objects of some mass:

$$\int_{-\infty}^\infty f_{\text{P-S}}(\sigma) d\ln \sigma^{-1} = 1. \quad (3)$$

The mass function $f(\sigma, z)$ is related to the number density, $dn(M, z)$, of haloes of mass M :

$$f(\sigma) \equiv \frac{M}{\rho_0} \frac{dn(M, z)}{d\ln \sigma^{-1}}, \quad (4)$$

where $\rho_0(z)$ is the mean comoving mass density.

The general agreement between the various simulated mass functions discussed earlier demonstrates, at least at an approximate level, the validity of the assumption that whether or not a region will collapse depends only upon its linear overdensity. These studies show that approximately equal mass is contained in haloes formed from fluctuations of equal rms linear overdensity, although these haloes may have different masses and redshifts, confirming the general “redshift invariance” of the mass function (Jenkins et al. 2001). However, in apparent contradiction, simulations of power law spectra ($P \propto k^n$) find that the shape of the mass function depends on spectral index, n (Efstathiou et al. 1988; Lacey & Cole 1994). This gives rise to the possibility that the cosmological mass function could depend on the local slope of the power spectrum, n_{eff} , which varies with scale, and thus, with halo mass.

Building upon P-S theory, Sheth & Tormen (1999) presented an improved mass function, which corresponds closely to that expected if one assumes haloes collapse as ellipsoidal rather than spherical structures (Sheth, Mo, & Tormen 2001):

$$f_{\text{S-T}}(\sigma) = A \sqrt{\frac{2a}{\pi}} \left[1 + \left(\frac{\sigma^2}{a\delta_c^2}\right)^p\right] \frac{\delta_c}{\sigma} \exp\left[-\frac{a\delta_c^2}{2\sigma^2}\right], \quad (5)$$

where $A = 0.3222$, $a = 0.707$ and $p = 0.3$. The S-T function matches numerical simulations over a wide range of masses and redshifts.

2.3 The mass function in a finite volume

Unfortunately, because of limitations in computational resources, simulations cannot follow evolution in volumes large enough to include physically relevant power on all scales while still maintaining adequate resolution. We are forced instead to infer the mass function of an infinite universe, i.e. the “true” mass function, from the numbers of haloes that form within a finite simulation volume assumed to be periodic. In order to use the numbers of simulated haloes to compute the true abundance of haloes that should be present within an infinite volume, we must understand the impact of finite box size on the simulated mass function. Previous authors (Power & Knebe 2005; Bagla & Prasad 2006) have noted that the effects of missing large-scale power can be estimated by imposing a cut-off for large-scale modes in the variance, as follows:

$$\sigma_{\text{box}}^2(M, z) \simeq \frac{b^2(z)}{2\pi^2} \int_{2\pi/L_{\text{box}}}^\infty k^2 P(k) W^2(k; M) dk. \quad (6)$$

Using Eq. 6 to relate halo mass and variance, the global mass function could then be estimated (see § 3.1 for further details), or the halo abundance expected from a finite volume could be computed using a selected analytic function. This approach approximately accounts for the lack of power at scales larger than the boxlength. However, the correction does not take into account the “cosmic variance” caused by the finite number of modes in a simulation, which causes each realization of a finite volume to have a unique mass function, as noted by Sirk (2005). This makes unclear the relation between the mass function of an individual simulation and the “true” value of the function for an infinite volume. Even in the limit of an infinite number of realizations of finite volumes, the discreteness imposed on scales near the box size will introduce errors into the inferred “true” mass function.

A better strategy for correcting for the effects introduced by the limited physical scale and number of modes is to employ the actual power spectrum used in the simulation, rather than the expectation value of Eqn. 1, in order to determine the relation between variance and mass. To compute the variance for our box, we first measure the mean power at each wavenumber present in the box, $\bar{P}(k)$, as measured from the initial particle distribution. Then we compute the following sum to determine the variance within the simulation volume:

$$\sigma_{\text{sim}}^2(M, z) = \frac{b^2(z)}{L_{\text{box}}^3} \sum_k N_{\text{modes}}(k) \bar{P}(k) W^2(k; M), \quad (7)$$

where N_{modes} is the number of modes that are present in the box for a particular wavenumber k . We later demonstrate the extent to which using this estimate of the variance in the simulation improves the inferred global mass function. This method produces the most significant improvement on small simulation volumes ($L_{\text{box}} \lesssim 100 \text{ h}^{-1}\text{Mpc}$), and has little effect for large volumes ($L_{\text{box}} \gg 100 \text{ h}^{-1}\text{Mpc}$). One should note that there still exists a “residual variance” due to the

random phases of waves in the density field of each realization. This implies that Poisson uncertainties are still an underestimation of the “true” errors, and that some correlation remains between the mass function in a particular bin with the mass function in neighbouring bins.

Some care must be taken in the measurement of the power spectrum from the initial particle distribution. At wavenumbers near the Nyquist frequency, the measurement is dominated by particle noise. However, since the number of modes in a box at small scales is high, the simulation power will be very close to the theoretical power, and the actual measured power is not needed near the Nyquist frequency. We thus adopt the theoretical power at scales below $20 \times$ the Nyquist frequency. We have estimated the power in the initial particle distribution using a cloud-in-cell mass assignment on a grid of twice the spatial resolution as the particles, the same as that used to estimate long range forces in L-GADGET2. These complications could be avoided if one instead used the actual power as drawn from the assumed Gaussian random distribution that each realization was intended to have – i.e., the Fourier-space amplitude of each density wave from which the real-space density fields are computed. However, we did not use this technique because this information is not available for all the simulations that we have analyzed.

3 RESULTS

3.1 The mass function

In Fig. 1, we show the simulation mass functions at redshifts ten, twenty, and thirty. The left panel simply shows the measured raw abundance of haloes within the (finite) simulation volumes. In the right panel, the global mass function is plotted including the transformation for the effect of finite volume, which utilizes the actual power spectrum of each random realization to derive the variance as a function of mass; i.e. we use $\sigma_{\text{sim}}^2(M)$ (Eqn. 7) rather than $\sigma_\infty^2(M)$ (Eqn. 1). This procedure involves adjusting the halo mass such that the variance within an infinite volume at the scale of the adjusted mass, M_a , is equal to the actual variance of each realization ($\sigma_\infty^2(M_a) = \sigma_{\text{sim}}^2(M)$), and then making the corresponding transformation to the abundance so as to satisfy the relation between collapsed fraction and abundance (Eqn. 4). For example, if $M_a = 2M$, then the abundance measured in the simulation is multiplied by a factor of $M/M_a = 0.5$ to yield the correct global abundance as plotted in the right panel of Fig. 1. This adjustment provides an estimate of the mass function our simulations would have produced if we had modelled an infinite volume. Because of the missing power in smaller volumes, the net effect is an increase in the mass and a decrease in the abundance of a given bin in such a way that the resulting adjusted mass function is higher at a given mass. Note that the variation between simulations is very much reduced and the agreement between different box sizes is much improved. Once this transformation has been made, the simulated mass function lies nearer, but generally below the Sheth-Tormen function for the most massive objects at redshift ten to thirty. The Press-Schechter mass function is a poor match to the simulation data, especially at high masses.

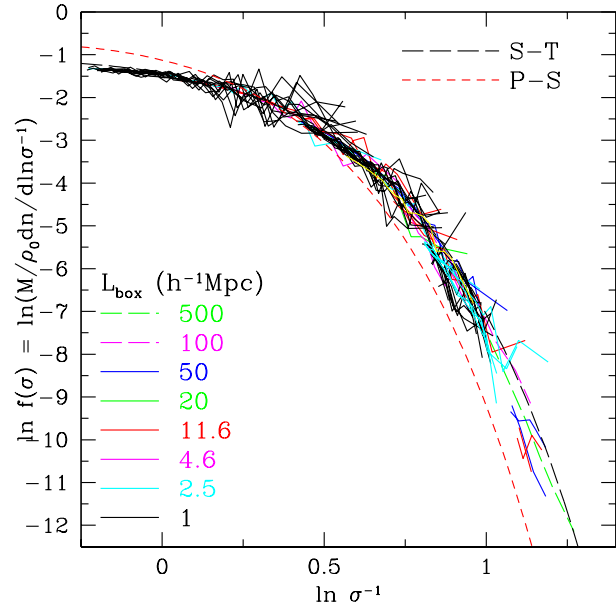


Figure 2. The fraction, $f(\sigma)$, of collapsed mass per unit $\ln \sigma^{-1}$, where σ^2 is the variance, at $z = 10, 20$, and 30 . The mass fraction has been adjusted to account for finite volume effects as described in § 2.2. Approximate redshift invariance is indicated by the fact that all redshifts have roughly the same mass function.

It is instructive to plot the fraction of collapsed mass as a function of inverse variance. This fraction is independent of redshift according to the principles underlying P-S or S-T models. In Fig. 2, we plot $f(\sigma)$ as a function of $\ln \sigma^{-1}$, including the correction for finite volume. The fact that the data over a wide range of redshifts all coincide approximately in a single form is an indication of the general redshift independence of the mass function. However, we discuss in § 3.2 some evidence for a weak dependence on redshift. Haloes formed from rare fluctuations – high mass, high redshift, or both – lie at large values of δ_c/σ and hence large $\ln \sigma^{-1}$. Here the mass function is steepest. Note that rarer haloes do not necessarily have lower spatial abundance. This can be understood by comparing a high redshift low mass halo with a low redshift high mass halo, each forming from e.g. a 5- σ fluctuation ($[\delta_c/\sigma(M, z)] = 5$). In the case of the low mass, high redshift halo, the number of regions per comoving volume element that contain the halo’s mass is larger, which results in a higher comoving halo abundance.

An important quantity is the cumulative fraction of mass contained in haloes. In Fig. 3, we plot the ratio of $f(> M)$ divided by the S-T function. In the right panel, the global mass function has been corrected using the actual power from each simulation in the relation between halo mass and variance (Eqn. 7), as in Fig. 1, which automatically accounts for finite volume effects. The greatly reduced run-to-run scatter compared to the raw, uncorrected mass function highlights the improvement gained by using a more accurate relation between halo mass and variance. The correction for limited simulation volume is evidenced by the systematic upward shift in the cumulative mass fraction, which is strongest for small boxes, and for high mass and/or redshift “rare” haloes.

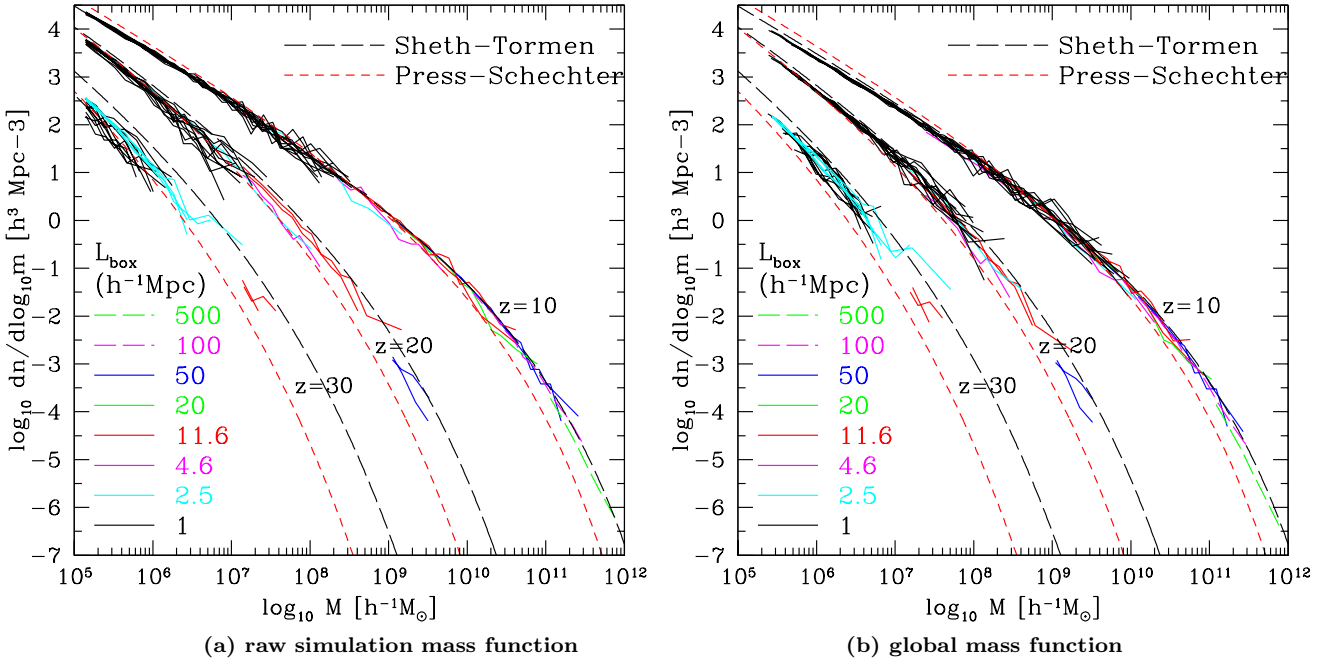


Figure 1. Differential simulated mass function of *friends-of-friends* dark matter halos for redshift 10, 20, and 30 compared with the Sheth & Tormen and Press & Schechter analytic predictions. The corrected mass function (right panel) makes a correction for cosmic variance and for finite volume to the simulation mass fluctuation spectrum by using the relation between σ^2 and mass derived from the power spectrum of the initial particle distribution for each realization; i.e. the left panel uses $\sigma_\infty^2(m)$ (Eqn. 1, the variance versus mass for an infinite universe) and the right panel utilizes $\sigma_{\text{sim}}^2(m)$ (Eqn. 7, the actual variance for each realization). Note the reduced run to run scatter and increased amplitude of the corrected mass functions for small boxes. For comparison purposes, the 100 and 500 $h^{-1}\text{Mpc}$ runs have been rescaled by the ratio of their expected S-T mass functions to account for their mildly different transfer functions.

3.2 Fitting the mass function

An analytic form for the mass function is an essential ingredient for a wide array of models of galaxy formation, reionization, and other phenomena, and is also required for cosmological studies based on observable objects whose number density depends on the halo mass function. In Fig. 4, we show our data along with several analytic functional fits; see also Fig. 5a-d, where we plot the mass function split by redshift. The error bars in Figs. 4-6 are obtained by computing the square root of the number of haloes in each mass bin.

The S-T function provides a reasonable fit except for rare haloes (large $\delta_c/\sigma(m, z)$), where the simulations produce $\sim 50\%$ fewer objects. The P-S function is a poor fit at all redshifts. Of the previously published fits, Reed et al. (2003) is the most consistent with our combined high and low redshift data, fitting the data with an rms difference of 11%, i.e. $\chi^2 = 1$ if we artificially set the uncertainties to be equal to the Poisson errors plus 11% of the measured abundance, added in quadrature. The Jenkins et al. function is an excellent fit to our low redshift simulation data, but it matches the high redshift data less well. This comparison, however, requires extrapolating the function beyond its intended range of validity, namely the original fitted range of $-1.2 < \ln \sigma^{-1} < 1.05$.² The Warren et al. (2005) curve,

² Due to differences in binning the data in the regime where the mass function is steep, we find the $z = 10$ mass function in the Millennium run (the six rightmost $z = 10$ points in Fig. 4) to

which is very similar to the Jenkins et al. form over its original fitted range, fits our lowest redshift data quite well, but it is not as good a fit to our high redshift results.

We now consider whether our data support an improved fit compared to published analytic mass functions. We define the effective slope, n_{eff} , as the spectral slope at the scale of the halo, where $P(k_h) \propto k_h^{n_{\text{eff}}}$ and $k_h = 2\pi/r_0$, with r_0 the radius that would contain the mass of the halo at the mean cosmic density. If we limit the fit to a redshift independent form, with the assumption of no dependence on n_{eff} , our simulation data can be fit by steepening the high mass slope of the S-T function (Eq. 5) with the addition of a new parameter, $c = 1.08$, in the exponential term, and simultaneously including a Gaussian in $\ln \sigma^{-1}$ centered at $\ln \sigma^{-1} = 0.4$, as described by the following function, which is otherwise identical to the S-T fit:

$$f(\sigma) = A \sqrt{\frac{2a}{\pi}} \left[1 + \left(\frac{\sigma^2}{a\delta_c^2} \right)^p + 0.2G_1 \right] \frac{\delta_c}{\sigma} \exp \left[-\frac{ca\delta_c^2}{2\sigma^2} \right] \quad (8)$$

$$G_1 = \exp \left[-\frac{(\ln \sigma^{-1} - 0.4)^2}{2(0.6)^2} \right]$$

The resulting function is comparable to the Reed et al. (2003) fit. Note that this modification means that the original normalization criteria – that all mass be contained in haloes, (Eqn. 3) – is not satisfied exactly; instead, 98%

be $\sim 10 - 20\%$ lower than in Springel et al. (2005), who found somewhat better agreement with the Jenkins et al. fit.

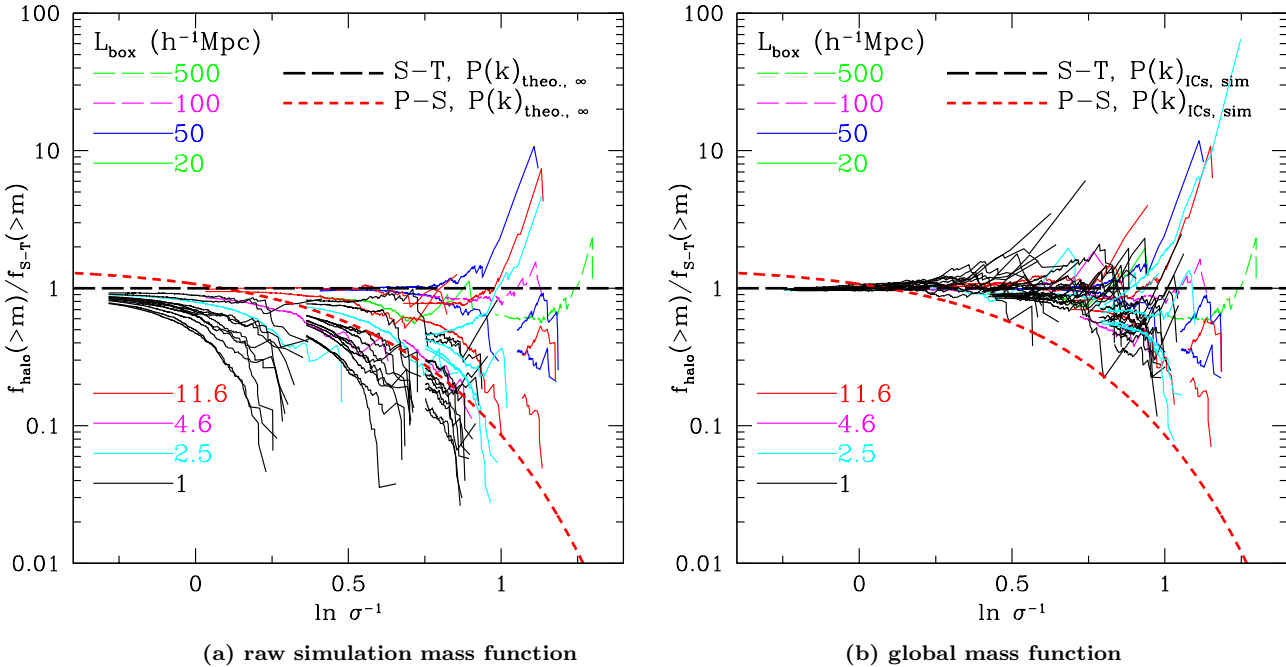


Figure 3. Cumulative fraction of mass contained in FOF haloes. Left panel assumes $\sigma_\infty(m)$ (Eqn.. 1), the variance for an infinite universe). Right panel utilizes $\sigma_{\text{sim}}(m)$ (Eqn. 7), the variance-mass relation derived from the mass power spectrum of the initial particle distribution. Accounting for missing large-scale power in this way results in the systematic upward shift in the corrected mass function. Reduced run-to-run scatter and improved agreement between different box sizes (different colors) indicates the effectiveness of the finite volume correction to the mass function.

of mass is contained in haloes. It is remarkable that our data at all redshifts over a vast range in masses are generally consistent with a single functional fit that is solely a function of the variance, independent of redshift. However, while this redshift independent function appears reasonable at high redshift, it is relatively poor at $z = 0$.

Careful inspection reveals tentative evidence for a dependence on some additional free parameter(s). The mass function at $z \geq 10$ is suppressed, at levels of $\gtrsim 10 - 20\%$, relative to lower redshifts, indicating a weak dependence of the mass function on redshift. However, since a given value of σ corresponds to different masses at different redshifts, it is unclear whether the apparent trend with redshift masks a dependence on mass or on some other parameter. Regardless of the cause, inclusion of an additional parameter in the mass function provides a better fit to our data, as we now show. We consider the possibility that the mass function may be affected by n_{eff} , the power spectral slope at the scale of the halo radius. An improved fit can be made at each redshift with the introduction of n_{eff} in the analytic function, as given by the following formula, again a modification to the S-T function:

$$f(\sigma, n_{\text{eff}}) = A \sqrt{\frac{2a}{\pi}} \left[1 + \left(\frac{\sigma^2}{a\delta_c^2} \right)^p + 0.6G_1 + 0.4G_2 \right] \quad (9)$$

$$\times \frac{\delta_c}{\sigma} \exp \left[-\frac{ca\delta_c^2}{2\sigma^2} - \frac{0.03}{(n_{\text{eff}}+3)^2} \left(\frac{\delta_c}{\sigma} \right)^{0.6} \right],$$

$$G_1 = \exp \left[-\frac{(\ln \sigma^{-1} - 0.4)^2}{2(0.6)^2} \right],$$

$$G_2 = \exp \left[-\frac{(\ln \sigma^{-1} - 0.75)^2}{2(0.2)^2} \right].$$

where $c = 1.08$, and G_1 and G_2 are gaussian functions in $\ln \sigma^{-1}$. This function fits the data to 4%rms accuracy, significantly better than the 15%rms accuracy of the single parameter fit of Eqn. 8.

The new analytic mass function is presented for redshifts zero through thirty in Fig. 5a-d. The broad ‘bump’ over the S-T function in the $z = 0$ mass function centered near $\ln \sigma^{-1} = 0.4$, which is also present in the Jenkins et al. and Warren et al. fits, is produced by the Gaussian functions in $\ln \sigma^{-1}$ space. The n_{eff} term introduces a redshift dependence that increasingly suppresses the mass function as n_{eff} approaches -3, and becomes stronger for rarer haloes. From Eqn. 1, it is easy to show that for a pure power-law fluctuation power spectrum, $\sigma^2 \propto M^{-(n_{\text{eff}}+3)/3}$, which can be reparameterized as

$$n_{\text{eff}} = 6 \frac{d \ln \sigma^{-1}}{d \ln M} - 3. \quad (10)$$

At fixed redshift, n_{eff} is thus a proxy for halo mass. At the smallest scales, the CDM power spectrum asymptotes to $n_{\text{eff}} = -3$ for a primordial spectral slope $n_s = 1$. We have computed n_{eff} using Eqn. 10 throughout this paper. However, for convenience, since n_{eff} is nearly linear with $\ln \sigma^{-1}$ over relatively small ranges in M , n_{eff} can be approximated to better than 10% in $(n_{\text{eff}} + 3)$ by the following function within the mass and redshift range of haloes in this paper and for $\sigma_8 = 0.9$:

$$n_{\text{eff}} \simeq m_z \ln \sigma^{-1} + r_z \quad (11)$$

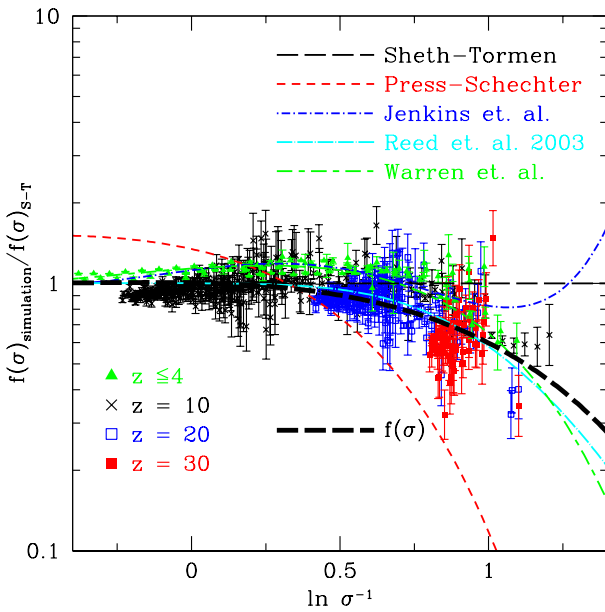


Figure 4. Differential global (corrected for finite volume; see text) mass function of *friends-of-friends* dark matter halos for redshift 0, 1, 4, 10, 20, and 30 compared with analytic fits. Thick curves correspond to the modified S-T function (Eq. 8). Error bars denote 1- σ poisson uncertainties.

$$m_z = 0.55 - 0.32 \left[1 - \left(\frac{1}{1+z} \right) \right]^5$$

$$r_z = -1.74 - 0.8 \left| \log \left(\frac{1}{1+z} \right) \right|^{0.8}.$$

In Fig. 6, we plot the ratio of the simulation data to the new analytic fits, with (panel b) and without (panel a) the n_{eff} dependence. The better fit obtained when n_{eff} is included suggests that the halo mass function is not redshift independent and thus cannot be described solely by the single parameter $\sigma(m, z)$. However, panel a) shows that any dependency on additional parameters is very weak. Nevertheless, the precise causes of this apparent dependency warrant further study.

4 SENSITIVITY TO COSMOLOGICAL PARAMETERS

Our general results are unaffected by the exact values of the cosmological parameters because the fit of the mass function in the simulations to an analytic form is, in principle, independent of the precise relation between variance and mass (although a dependence on n_{eff} introduces a weak dependence on cosmological parameters through the relation between n_{eff} and $\sigma(m, z)$). Studies involving a wide range of cosmological parameters (e.g. Jenkins et al. 2001; White 2002) have ruled out a strong dependence of $f(\sigma)$ on matter or energy density. This allows one to estimate the halo abundance for a range of plausible cosmological parameters using purely the analytic mass function determined by $\sigma(m, z)$. In particular, the third year WMAP results (WMAP-3), which confirm the analysis by Sanchez et al. (2006) of the first year

WMAP and other CMB experiments combined with the 2dFGRS, imply a fluctuation amplitude significantly smaller than is commonly assumed, and also suggest a spectral index smaller than 1. Both of these parameters have a significant impact on the number of small haloes at high redshift.

Figs. 7 and 8 show that, compared to the cosmology assumed in the rest of this paper ($\sigma_8 = 0.9$, $n_s = 1.0$, $\Omega_m = 0.25$), the cosmological parameters inferred from the WMAP-3 data imply a factor of 3 decrease in the number of candidate galaxy hosts at $z = 10$ with mass $\sim 10^8 h^{-1} M_\odot$, and nearly three orders of magnitude decrease in the number of potential galaxies at $z = 30$ with mass $\sim 2 \times 10^7 h^{-1} M_\odot$. Smaller “mini-haloes” which could host population III stars are also strongly affected. The WMAP-3 cosmology implies one third fewer “mini-haloes” of mass $\sim 10^6 h^{-1} M_\odot$ at $z = 10$ and a reduction by more than two orders of magnitude at $z = 30$ relative to our standard cosmology. Note that the comoving abundances in Fig. 7 do not match exactly the values in Fig. 1 because a slightly different transfer function was used for some of the simulations, as discussed in §2.1.

The effect of the WMAP-3 cosmological parameters can also be interpreted either as reducing the mass of typical haloes at a given redshift, or as introducing a delay in the formation of structure. For example, haloes with number density $1 h^3 \text{Mpc}^{-3}$ at $z = 10$ would have a mass approximately 2.5 times larger in our standard cosmology than in the WMAP-3 cosmology; for the same fixed number density, this becomes a factor of ~ 4 at $z = 20$ and a factor of ~ 6 at $z = 30$. For haloes of a fixed mass, the reduced σ_8 and n_s of the WMAP-3 cosmology delay halo formation. For example, haloes of mass of $10^8 h^{-1} M_\odot$ are delayed by $\Delta z \simeq 4$ ($z=21$ to $z=17$) before reaching a comoving abundance of $10^{-2} h^3 \text{Mpc}^{-3}$. Haloes of $10^6 h^{-1} M_\odot$, approximately the mass where H₂-cooling becomes strong enough to trigger star formation, do not reach an abundance of $1 h^3 \text{Mpc}^{-3}$ until $z = 24$ for the WMAP-3 cosmology compared to $z = 30$ for our standard cosmology. This means that widespread population III star formation and galaxy formation would occur significantly later if the WMAP-3 cosmological parameters were correct.

The uncertainties that remain in the values of cosmological parameters translate into significant uncertainties in the number of high redshift haloes that can potentially host luminous objects, especially those haloes that host the first generations of stars and galaxies. This adds major uncertainty to predictions of the abundance of potentially detectable haloes in the pre-reionized universe, such as those modeled in e.g. Reed et al. (2005). However, the sensitivity of halo number density to cosmological parameters suggests the exciting prospect of using the number of small haloes at high redshift as a cosmological probe if future studies are able to establish their number density accurately.

5 DISCUSSION

Our simulations give the mass function of dark matter haloes out to redshift 30 and down to masses that include the smallest haloes likely to form stars, “mini-haloes” whose baryons collapse through H₂ cooling. Thus, we now have a precise estimate of the mass function of the halos that contain all

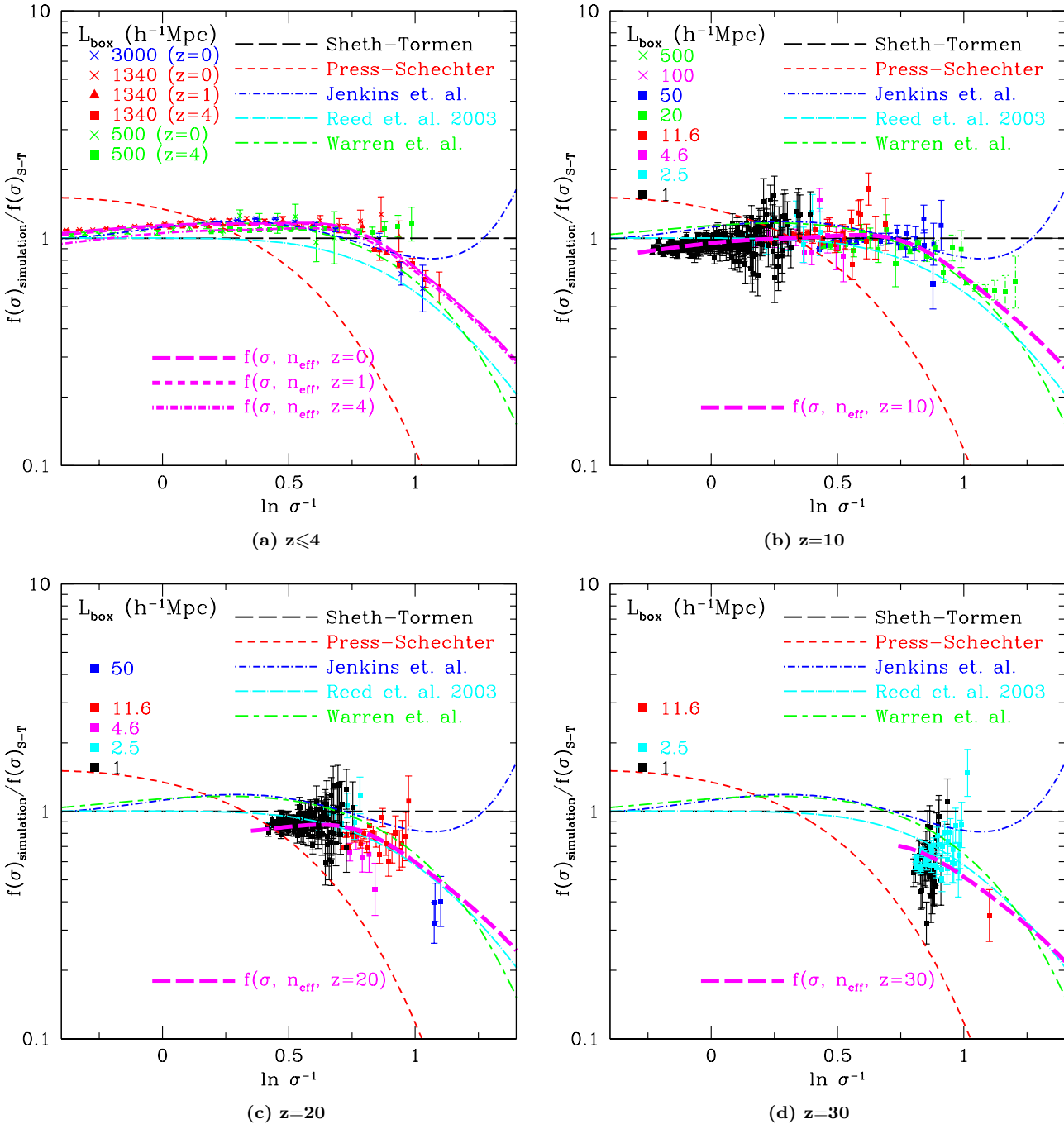


Figure 5. Differential global (corrected for finite volume; see text) mass function of *friends-of-friends* dark matter halos for redshift 10, 20, and 30 compared with analytic fits, including our new two-parameter fit (Eqn. 12), which includes a dependence on spectral slope, n_{eff} , and the resulting redshift dependence.

the stellar material at observable redshifts, and at virtually all the redshifts that are potentially observable in the foreseeable future. Our fits were obtained using simulations of the Λ CDM cosmology for a specific set of cosmological parameters, but they are readily scaleable to other values.

These haloes may be detected in a numbers of ways. Large haloes (those with $T_{vir} > 10^4$ K), which have the potential to host galaxies formed by efficient baryon cooling, might be observed out to the epoch of reionization with the

JW Space Telescope, or perhaps even with current generation infrared observatories. Smaller haloes may not be directly observable. However, their stellar end-products might, as gamma-ray bursts (e.g. Gou et al. 2004), or as supernovae at redshifts well above the epoch of reionization (e.g. Weinmann & Lilly 2005).

Knowledge of the halo mass function will be important in the interpretation of data from the Low Frequency Array (LOFAR), the Square Kilometer Array (SKA) or other

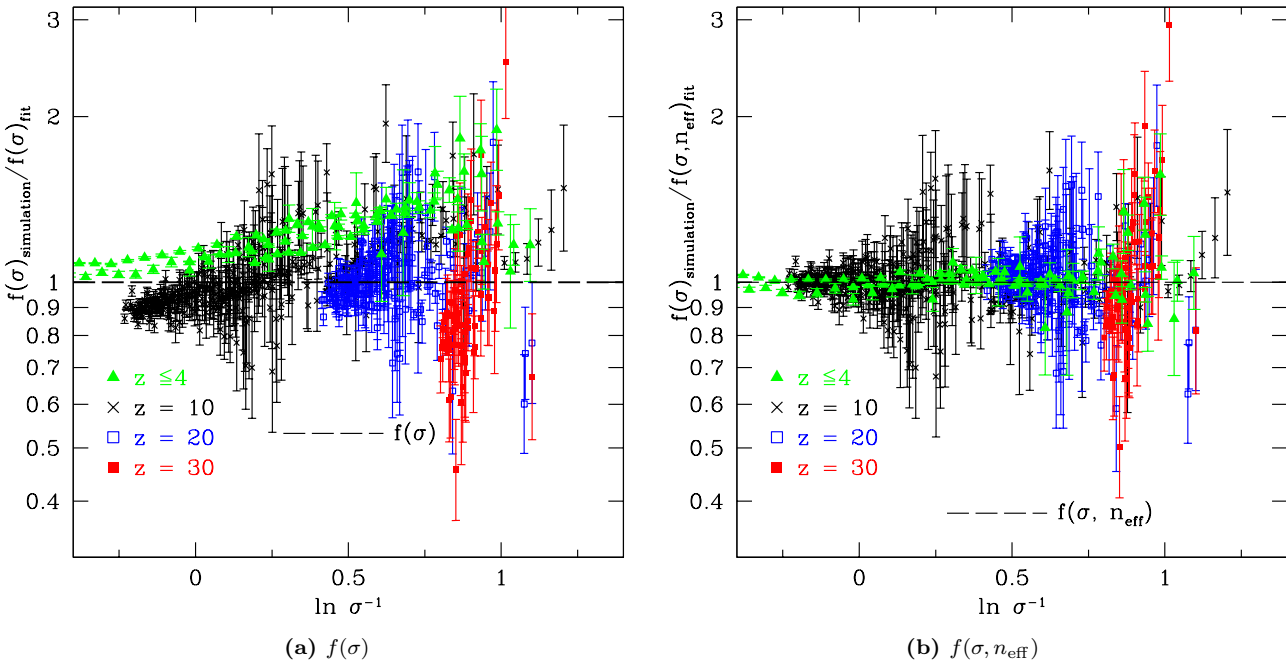


Figure 6. Ratio between the differential global (corrected for finite volume; see text) mass function of *friends-of-friends* dark matter halos at redshift 0, 1, 4, 10, 20 and 30, and our single parameter fit (left; Eqn. 8); ratio between the same simulation data and a new fit that includes n_{eff} as a second parameter (right; Eqn. 12). The improved fit in the right panel shows that our results are better described by a two-parameter function, rather than simply a function of $\ln \sigma^{-1}$. This is evidence for a weak redshift dependence (via n_{eff}) of the mass function.

rest-frame 21cm experiments designed to discover and probe the epoch of reionization. It may even be possible to use the halo mass function to help break degeneracies between cosmological parameters and the astrophysical modelling of the first objects.

Our results for the halo mass function at high redshift imply that predictions for the abundance of dark matter haloes that may host galaxies, stars, gamma-ray bursts or other phenomena based on the commonly used Press-Schechter model grossly underestimate the number of 3σ or rarer haloes. This includes large galaxies at $z \sim 10$, all haloes large enough to host galaxies at $z \gtrsim 15$, and all haloes capable of hosting stars at $z \gtrsim 20$, assuming that a halo must be at least $\sim 10^8 h^{-1} M_\odot$ to host a galaxy and $10^6 h^{-1} M_\odot$ to form stars. The P-S function underestimates the true mass function by a factor ~ 5 for the rarest haloes that we have simulated, which applies to galaxy candidates at $z = 30$, and large ($\sim 10^{11} h^{-1} M_\odot$) galaxies at $z = 10$. The abundance of mini-haloes likely to host Population III stars are underestimated by the P-S function by a factor of at least two at $z = 30$. Studies that assume the Sheth & Tormen function are more robust, but they still suffer from an overestimation of the numbers of large haloes at high redshift, particularly of large galaxies at $z \gtrsim 10$, extending to all potential galaxies at $z \gtrsim 20$, and to all star-forming haloes at $z \gtrsim 30$, reaching a factor of up to ~ 3 for the rarest haloes in our simulations. However, the S-T function overpredicts the number of mini-haloes only by less than $\sim 20\%$ at $\lesssim 20$ and by $\sim 40\%$ at $z = 30$.

6 SUMMARY

We have determined the mass function of haloes capable of sustaining star formation from redshift 10 to 30, a period beginning well before reionization and extending to redshifts below those where reionization occurred according to the WMAP 3-year estimates. This extends the mass function to lower masses and higher redshifts than previous work, and includes the ‘‘mini-haloes’’ that probably hosted population III stars. Our main results may be summarized as follows:

- We have presented a novel method for correcting for the effects of cosmic variance and unrepresented large-scale power in finite simulation volumes. This allows one to infer more accurately the true global mass function, ultimately allowing the mass function to be computed to smaller masses. We have verified the robustness of this method by carrying out simulations of a wide range of volumes and mass resolutions and comparing the inferred mass functions for overlapping halo mass ranges. By simulating multiple realizations of identical volumes, we show that the run-to-run scatter in the mass function, caused by cosmic variance, is minimized by our method.
- Throughout the period $10 < z < 30$, the halo mass function is broadly consistent with the Sheth & Tormen (1999) model for haloes 3σ and below. For rarer haloes, the mass function drops increasingly below the S-T function – by up to $\sim 50\%$ for $\sim 5\sigma$ haloes.
- Our data are reasonably well fit by a redshift-independent function of $\sigma(m, z)$, the rms linear variance in top hat spheres. We provide a 1-parameter fit to the mass function which is a modified version of the Sheth & Tormen (1999) formula. However, an even better fit can be obtained if

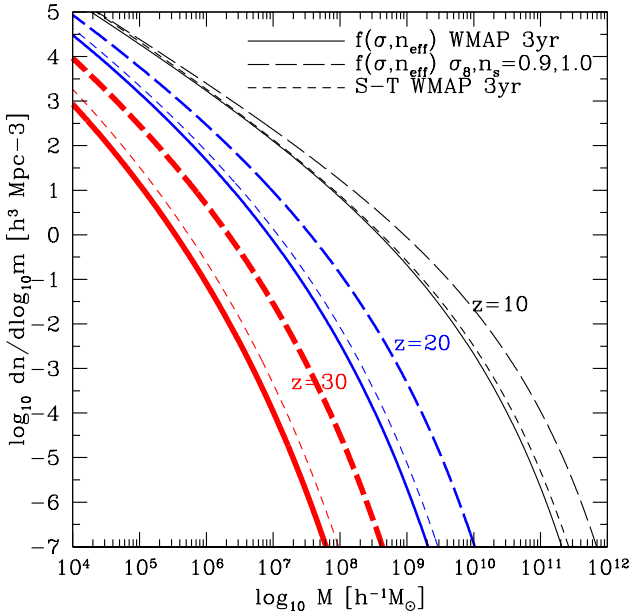


Figure 7. Differential analytic mass function for the WMAP 3-year cosmological parameters (Spergel et al. 2006), compared with the mass function for the standard cosmological parameters assumed in the simulations of this work. The curves marked ‘‘WMAP 3yr’’ use the preferred WMAP 3-year parameters (e.g. $\sigma_8, n_s = 0.74, 0.951$), including the effect of the preferred parameters (e.g. $\Omega_m, \Omega_{baryon}$, etc) on the transfer function. The abundance of massive, high redshift haloes is highly sensitive to cosmological parameters due to the steepness of the mass function.

the mass function is allowed to depend not only on $\sigma(m, z)$, but also on the slope of the primordial mass power spectrum, n_{eff} . This improvement implies that the fraction of collapsed mass does not depend solely on the rms linear overdensity, as is assumed in Press-Schechter theory. The P-S formula, in fact, provides a poor fit to most of our data.

- The halo abundance at $z \gtrsim 10$ is highly sensitive to σ_8 and n_s , parameters recently adjusted downwards in the reported WMAP 3-year results (Spergel et al. 2006). The new estimates imply greatly reduced numbers of high redshift haloes of a given mass. The sensitivity of high-redshift halo numbers to these parameters suggests their potential as a useful cosmological probe in future.

ACKNOWLEDGMENTS

We thank Raul Angulo for providing halo catalogs for the 1340 h^{-1} Mpc simulation. DR is supported by PPARC. RGB is a PPARC Senior Fellow. TT thanks PPARC for the award of an Advanced Fellowship. The simulations were performed as part of the simulation programme of the Virgo consortium. The new simulations introduced in this work were performed on the Cosmology Machine supercomputer at the Institute for Computational Cosmology in Durham, England.

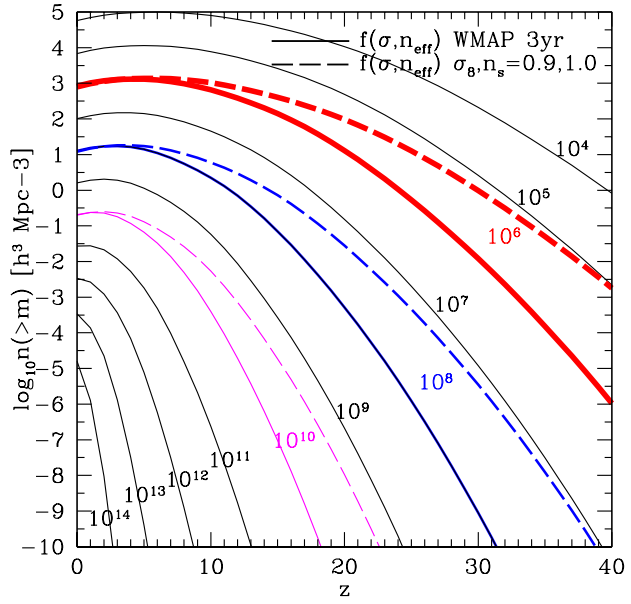


Figure 8. Cumulative abundance versus redshift for the WMAP 3-year cosmological parameters (Spergel et al. 2006) implied by our new analytic mass function (Eqn. 12). Also shown is the abundance of haloes for the standard cosmological parameters assumed in the simulations of this work for 3 masses. The curves are labeled by mass in units of $h^{-1}M_\odot$. The curves marked ‘‘WMAP 3yr’’ assume the complete preferred WMAP 3-year parameters ($\sigma_8, n_s = 0.74, 0.951$), including the effect of the preferred parameters (e.g. $\Omega_m, \Omega_{baryon}$, etc) on the transfer function. The abundances at high redshift are most sensitive to cosmological parameters.

REFERENCES

- Abel T., Bryan G., Norman M. L., 2000, ApJ, 540, 39
- Abel T., Bryan G., Norman M. L., 2002, Science, 295, 93
- Bagla J., Ray S., 2005, MNRAS, 358, 1076
- Bagla J., Prasad J., 2006, astro-ph/0601320
- Barkana R., Loeb A., 2004, ApJ, 609, 474
- Bond J., Efstathiou G., 1984, ApJ, 285, 45
- Bromm V., Coppi P. S., Larson R. R., 1999, ApJ, 527, L5
- Bromm V., Coppi P. S., Larson R. R., 2002, ApJ, 564, 23
- Bromm V., Larson R., 2004, ARA&A, 42, 79
- Ciardi B., Ferrara A., 2005, Space Science Reviews, 116, 625
- Colberg J., et al., 2000, MNRAS, 319, 209
- Couchman H., Thomas P., Pearce F., 1995, ApJ, 452, 797
- Davis, M., Efstathiou, G., Frenk, C.S., White, S.D.M., 1985, ApJ, 292, 381
- Efstathiou G., Frenk C. S., White S. D. M., Davis M., 1988, MNRAS, 235, 715
- Gao L., White S. D. M., Jenkins A., Frenk C. S., Springel V., 2005, MNRAS, 363, 379
- Gou L., Meszaros P., Abel T., Zhang B., 2004, ApJ, 604, 508
- Heitmann K., Lukic Z., Habib S., Ricker P., 2006, ApJ, 624, 85
- Jenkins A., Frenk C. S., White S. D. M., Colberg J., Cole S., Evrard A., Couchman H., Yoshida N., 2001, MNRAS, 321, 372

Lacey C., Cole S., 1993, MNRAS, 262, 627
 Lacey C., Cole S., 1994, MNRAS, 271, 676
 Monaco P., Theuns T., Taffoni G., Governato F., Quinn T., Stadel J., 2002, ApJ, 564, 8
 Monaco P., Theuns T., Taffoni G., 2002, MNRAS, 331 587
 Pearce F., Couchman H., 1997, NewA, 2, 411
 Peebles P., 1993, Principles of Physical Cosmology, Princeton Univ. Press, Princeton, NJ, USA
 Power C., Knebe A., 2005, astro-ph/0512281
 Press W.H., Schechter P., 1974, ApJ, 187, 425
 Reed D., Gardner J., Quinn T., Stadel J., Fardal M., Lake G., Governato F., 2003, MNRAS, 346, 565
 Reed D. S., Bower R., Frenk C.S., Gao L., Jenkins A., Theuns T., White S.D.M., 2005, MNRAS, 363, 393
 Sanchez A., Baugh C., Percival W., Peacock J., Padilla N., Cole S., Frenk C., Norberg P., 2006, MNRAS, 366, 189
 Schneider R., Salvaterra R., Ferrara A., Ciardi B., 2005, astro-ph/0510685
 Seljak U., Zaldarriaga M., 1996, ApJ, 469, 437 S
 Sheth R., Mo H., Tormen G., 2001, MNRAS, 323, 1
 Sheth R., Tormen G., 1999, MNRAS, 308, 119
 Sirko E., 2005, ApJ, 634, 728
 Spergel D., et al. , 2003, ApJS, 148, 175
 Spergel D., et al. , 2006, astro-ph/0603449
 Springel V., 2005, MNRAS, 364, 1105
 Springel V., et al. , 2005, Nature, 435, 629
 Warren M., Abazajian K., Holz D., Teodoro L., 2005, astro-ph/0506395
 Weinmann S., Lilly S., 2005, ApJ, 624, 526
 White M., 2002, ApJS, 143, 241
 White S. D. M., Springel V., 2000, “Where are the first starts now?”, The First Stars, Proceedings, eds Weiss A., Abel T., & Hill V., Springer, p. 327
 Zel'dovich Y., 1970, A&A, 5, 84

APPENDIX A: NUMERICAL TESTS

A1 Run parameter convergence tests

In Fig. A1, we have tested some of the primary runtime parameters of L-Gadget2 using a $10^3 h^{-1} M_\odot$ particle resolution $1 h^{-1} \text{Mpc}$ volume. These tests confirm that our choices of starting redshift (z_{start}), fractional force accuracy ($\Delta_{\text{force acc}} = 0.005$), softening length (r_{soft}), and maximum allowed timestep ($\Delta t = \Delta \ln(1+z)^{-1}$) are sufficient. Of the parameters that we have tested, z_{start} has the most effect on our results. At $z=10$, $z_{\text{start}} = 119$ is indistinguishable from earlier starting redshifts. However, at $z=20$, the $z_{\text{start}} = 119$ mass function is suppressed by $\sim 10 - 20\%$ relative to the $z_{\text{start}} = 299$ runs, and by more than 50% at $z=30$. At $z=30$, the $z_{\text{start}} = 299$ run is suppressed relative to the $z_{\text{start}} = 599$ run by $\sim 10 - 20\%$, which could indicate a small bias in our $z=30$ mass function, but not large enough to affect significantly our conclusions. It thus appears that a simulation must be evolved a factor of ~ 10 in expansion factor in order to solve accurately (within 10-20%) the mass function for the mass resolutions and outputs we have considered.

A2 Resolving haloes

Studies of the mass function at low redshift have found that the mass function is adequately sampled for haloes containing as few as 20 particles (e.g. Jenkins et al. 2001). Because we are exploring new regimes in mass and redshift, it is necessary to confirm that we model haloes with sufficient particle numbers to resolve the mass function. The FOF mass function for haloes of very few particles is typically enhanced artificially as spurious groupings are increasingly common for small particle numbers.

Our resolution tests consists of an identical volume, simulated at multiple mass resolutions. The mass function of a $2.5 h^{-1} \text{Mpc}$ box at resolutions of 200^3 , 500^3 , and 1000^3 is shown in Figure A2. At each resolution, the mass function has an upturn below approximately 30-40 particles. Additionally, the mass function is suppressed over the range of ~ 30 to ~ 100 particles, at a level that appears to depend on redshift. At scales larger than approximately 100 particles, the mass function at multiple resolutions agrees within the uncertainties. For this reason, we limit our analysis to haloes of at least 100 particles. This resolution limit is significantly higher than found necessary at low redshift in many previous works. Even with this conservative particle resolution limit, some small bias in the mass function cannot be ruled out fully for redshifts 20 or higher. The increased sensitivity of the mass function to particle resolution as redshift increases is likely enhanced by the increased steepness of the mass function in this regime for haloes formed from rare fluctuations. The suppression of the mass function for haloes of fewer than 100 particles may be due to transient effects that become unimportant by lower redshifts. These effects could include errors introduced as a result of inaccuracies of the Zel'dovich approximation (Zel'dovich 1970) where initial particle positions and velocities are computed based on the initial density field, which is assumed to be entirely linear. Further investigation is required to determine more fully the sources of increased sensitivity to mass resolution on the mass function.

A3 Halo finders: friends-of-friends (FOF) versus spherical overdensity (SO)

Choice of halo finder can have a major impact on halo masses and on the mass function. It is thus worth considering how our results would change had we used a different halo finder. In this case, the FOF mass function is compared with the mass function produced by the *spherical overdensity* SO algorithm (Lacey & Cole 1994), which identifies spheres of a specified overdensity. FOF is computationally efficient and will select objects of any shape provided that they meet a local particle density. However, FOF may also spuriously link together neighbouring haloes, which is a potential issue for low mass, high redshift haloes which form at scales where mass fluctuation spectrum is steep, and result in highly ellipsoidal halo shapes (Gao et al. 2005). Because SO assumes haloes are spheres, it is not ideal for highly ellipsoidal haloes. However, SO has an advantage over FOF in that it is less likely spuriously to link together neighbouring haloes or to misclassify highly ellipsoidal but unvirialized structures as haloes.

We have tested the SO algorithm assuming the spherical

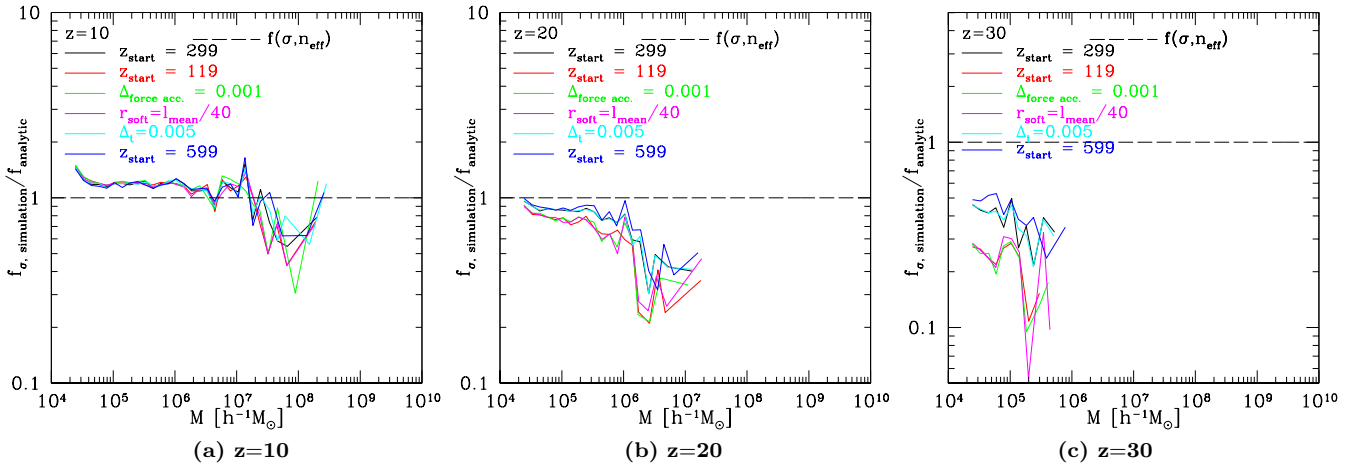


Figure A1. Differential raw (unadjusted for finite volumes) simulated mass function of *friends-of-friends* dark matter halos for redshifts 10, 20, and 30 is shown for several run parameters. Unless otherwise noted, each run used the parameters implemented throughout this paper ($z_{\text{start}} = 119$, $\Delta_{\text{force acc.}} = 0.005$, $r_{\text{soft}} = l_{\text{mean}}/20$, $\Delta_t = 0.02$), except that the green ($\Delta_{\text{force acc.}}$), and magenta (r_{soft}) curves used $z_{\text{start}} = 119$. Here haloes are plotted down to 20 particles per halo versus the 100 particle minimum imposed throughout the paper; particle mass is $1.1 \times 10^3 h^{-1} M_\odot$.

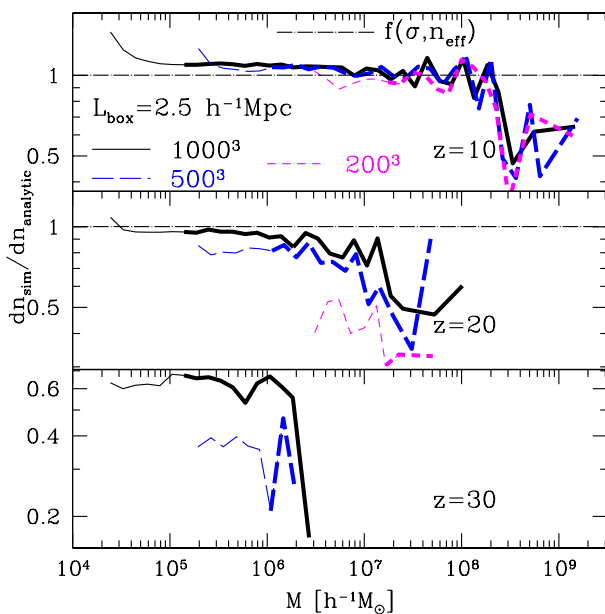


Figure A2. Residuals of the differential raw (unadjusted for finite volumes) mass function for a $2.5 h^{-1} Mpc$ box with identical initial density fluctuations modeled at 3 different mass resolutions (200^3 , 500^3 , and 1000^3 particles). Thick line segments denote haloes of at least 100 particles, the minimum particle number that we implement throughout the paper. Thin line segments show the mass function down to 20 particles per halo.

tophat model, in which the Λ CDM virial overdensity, Δ_{vir} , in units of the mean density is 178 at high redshifts, when $\Omega_m \simeq 1$. We have computed the SO mass function for three simulations of particle mass resolution $\sim 10^3$, 10^5 , and $10^7 h^{-1} M_\odot$ at redshifts 10, 20, and 30. In Figure A3, we show the SO and FOF mass functions for these outputs. In general, the SO mass function is lower than the FOF mass function,

though the two mass functions are consistent for much of the redshift 10 mass range. The difference between the two mass functions increases with mass and redshift, ranging from $\lesssim 10\%$ at redshift 10 and is generally less than a factor of 2. Some caution should be taken when considering the SO mass function because of its particle number dependence in this implementation of the SO halo finder. Initial candidate centers for SO haloes were identified by finding density peaks, where local density was computed for each particle, smoothed by its 32 nearest neighbours. Spheres were then grown outward until the desired overdensity was reached. This means that SO haloes with masses approaching and below the 32 particle smoothing mass will be suppressed.

While there are some differences in the mass function for the two means of identifying haloes, these differences are generally smaller than the differences introduced by adopting the WMAP 3 year cosmological parameters versus the larger $\sigma_8 = 0.9$ and $n_s = 1.0$ used in the simulations of this paper.

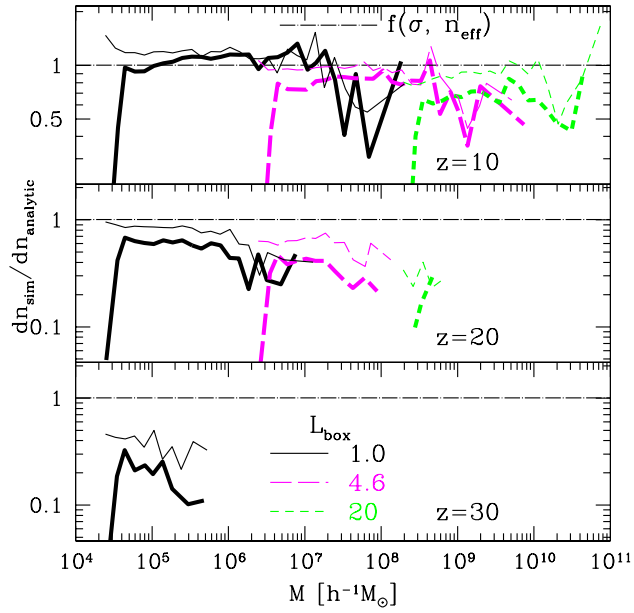


Figure A3. *friends-of-friends* (FOF, thin lines) and *spherical* overdensity (SO, thick lines) halo differential raw (unadjusted for finite volumes) mass functions for particle masses of $\sim 10^3$, 10^5 , and $10^7 h^{-1} M_\odot$ (box size of 1.0, 4.6, and $20 h^{-1} Mpc$ with 400^3 particles). For convenience, the differential mass functions are normalized to the Sheth-Tormen function. SO density is 178 times the mean density. Curves are plotted down to 20 particles per halo.